Built Heritage

RESEARCH ARTICLE

Open Access

Hygrothermal response of masonry facades with vapour-tight or capillary-active internal insulation under current and future climate scenarios

Xinyuan Dang[1*], Evy Vereecken[1,2], Hans Janssen[1] and Staf Roels[1]

Abstract

Interior thermal insulation has been widely used to improve energy efficiency and indoor comfort of historic buildings. However, traditional vapour-tight insulation materials strongly influence the hygrothermal behaviour of facades, which may lead to moisture-related problems. Capillary-active insulation aims to enhance moisture permeance, ensuring the hygrothermal response of the masonry wall is more aligned with that of an uninsulated wall. While some capillary-active systems have proven their efficiency, global climate change and extreme weather conditions introduce additional uncertainties. This study investigates this specific issue. The hygrothermal responses of three massive masonry walls — one with vapour-tight insulation, one with capillary-active insulation, and one uninsulated — are monitored and simulated under real climate conditions in Leuven, Belgium. The simulations, conducted in DELPHIN 6 with monitored climate datasets as boundary conditions, are validated using measured temperature and relative humidity. The validated model is subsequently used with one current and two future climate datasets to compare the impacts of vapour-tight and capillary-active insulation on the hygrothermal behaviours of the masonry walls under climate change. The former exhibited more serious moisture-related risks, offering only marginally better energy performance, while the latter showed a similar hygrothermal behaviour to the uninsulated wall. Exterior climates significantly influence hygrothermal responses: both insulation systems inevitably increase mould growth and frost damage risks, though moisture failures are reduced in warmer outdoor environments. This paper highlights the nuanced balance between energy efficiency and moisture safety for researchers and practitioners.

Keywords Hygrothermal simulation, Internal insulation, Climate change, Masonry façade, Capillary-active insulation, Vapour-tight insulation

1 Introduction

Thermal upgrading of building envelopes is crucial for renovating and retrofitting historic buildings, usually aiming to improve building energy efficiency (Lassandro and Turi 2017) and indoor thermal comfort (Lisitano et al. 2021). Interior insulation is often the only option when balancing historic facade conservation and building performance upgrade (Harrestrup and Svendsen 2015; Héberlé and Julien 2016; Biseniece et al. 2017; Hamid and Wallentén 2017; Walker and Pavía 2018; Blumberga et al. 2016). However, this standard solution may yield negative effects, for instance, summer overheating (Stazi et al. 2013) or moisture failures (Rose 2005; Lång et al. 2018), including interstitial condensation, mould growth, frost damage, etc. Illustratively, excessive moisture can

*Correspondence:
Xinyuan Dang
xinyuan.dang@kuleuven.be; dangxinyuan1994@gmail.com
[1] KU Leuven, Department of Civil Engineering, Section of Building Physics and Sustainable Design, Leuven 3001, Belgium
[2] Royal Institute for Cultural Heritage (KIK-IRPA), Monuments and Monumental Decoration Lab, Brussels 1000, Belgium

highly reduce the compression, shear, and bond strengths of masonry (Sathiparan and Rumeshkumar 2018), while interstitial condensation may also trigger chronic moisture accumulation (Klõšeiko et al. 2015), frost damage (Vereecken et al. 2015) and biological growth (Sedlbauer 2001; Dang et al. 2019; Li et al. 2020).

Hygrothermal properties of the applied insulation materials strongly govern the building performance and environmental risks. Traditional vapour-tight insulation materials, such as extruded polystyrene (XPS) and foam glass, restrict the inward vapour flow, thereby increasing the moisture content of the original wall. This condition may result in moisture-related problems (Klõšeiko and Kalamees 2022). To tackle this issue, capillary-active insulation materials, such as calcium silicate board (CSB) and wood fibre board, have been developed to facilitate moisture flow and hence reduce the risks of moisture failures (Grunewald, Ruisinger, and Häupl 2020; Ecological Building Systems[1]; Pukkapartners[2]; Casiplus[3]). A wide spectrum is observed in the hygric properties among so-called 'capillary-active' materials, of which some proved to be scarcely moisture permeable in lab tests (Vereecken and Roels 2016; Dang, Janssen, and Roels 2023a, 2024b).

Wind, rain, solar radiation, and other meteorological factors also exert a considerable influence on the hygrothermal response of building facades (Abuku et al. 2009; Dang et al. 2024a). Different climatic conditions necessitate case-specific approaches to the materials and thicknesses of the insulation systems to balance energy efficiency and heritage conservation (Zhu, Huckemann, and Fisch 2011; Berardi 2017; Yuan et al. 2017; Lalesca et al. 2019; Rosas-Flores and Rosas-Flores 2020; Huang et al. 2020). Global climate change and extreme weather hence constitute additional challenges in implementing boundary conditions (Drdácký 2010; Curtis 2010; Tingley 2015; Nik 2017; Dang et al. 2024a).

Numerical heat, air, and moisture (HAM) models are commonly employed for predicting the hygrothermal responses of building components (Delgado et al. 2012) based on material properties and boundary conditions as obtained from measurements (Dang, Janssen, and Roels 2024a, 2024b). Certain commercial HAM models provide built-in material properties databases, which have been measured and implemented by the model developers. These models also include climate datasets corresponding to a reference year at specific locations or the engineering conditions defined in standards, as well as surface transport coefficients and other factors which may consist of empirical values or default values in standards.

Nevertheless, material properties of historic building components exhibit a broad spectrum due to differences in prior production and exposure (Erkal et al. 2012; Vitiello, Castelluccio, and Merino 2020), while insulation materials vary significantly in hygrothermal transport and storage properties (Vereecken and Roels 2016; Bottino et al. 2019; Posani, Veiga, and de Freitas 2021; Dong et al. 2023; Dang, Janssen, and Roels 2023a, 2024b). Although users can implement specific measured or translated data as inputs, inaccuracies may still appear due to uncertainties in the inherent algorithms and/or customised assignments (Dang, Janssen, and Roels 2024b, 2025a; Dang et al. 2025b). Consequently, the deviations between the actual and implemented boundary conditions and material properties greatly influence the predicted performance of internal insulation systems.

More concerns need to be addressed when comparing the hygrothermal performance of historic masonry walls with vapour-tight and capillary-active insulation materials under climate change. Although sensitivity analyses have been conducted on various entries of identical insulation materials with different hygrothermal properties due to different manufacturers or batches and/or under varying weather scenarios in HAM models (Zhou et al. 2020; Lu et al. 2021; Panico et al. 2023; Janssens et al. 2024; Vandemeulebroucke et al. 2024; Gan et al. 2025), there remains a pressing need for in-depth understanding of both the hygrothermal properties of insulation materials and the implications under climate change.

This empirical study investigates the hygrothermal performance of masonry walls with different internal insulation systems under current and future climate scenarios. It is based on a dedicated full-scale dataset of test wall sections with (1) vapour-tight internal insulation, (2) capillary-active internal insulation, and (3) no insulation. XPS and CSB are applied as typical vapour-tight and capillary-active insulation materials. The three wall sections belong to the massive masonry facades of the experimental VLIET-building in Leuven, Belgium (Blocken and Carmeliet 2007; Desta, Langmans, and Roels 2011; Langmans 2016; Vereecken et al. 2020; Vereecken and Roels 2021a, 2021b; Dang et al. 2024a), whose monitored meteorological datasets in 2019 are used as boundary conditions and validation benchmarks for the simulation model in the numerical hygrothermal simulation model, DELPHIN 6. Three weather datasets (one current scenario and two future scenarios) regenerated

[1] See Redstone Calsitherm Climate Board on Ecological Building Systems website. https://www.ecologicalbuildingsystems.com/product/calsitherm-climate-board. Accessed April 24 2024.

[2] See 'Calcium silicate as insulation material for green buildings' on Pukkapartners website. https://www.pukkapartners.com/insight/calcium-silicate-as-insulation-material-for-green-buildings. Accessed 24 April 2024.

[3] See 'Technische Daten der Kalziumsilikatplatten' on Casiplus website. https://www.casiplus.de/technische-daten. Accessed 24 April 2024.

by the OCCuPANt project (Doutreloup and Fettweis 2021; Doutreloup et al. 2022) are later imposed to the validated model for evaluating the hygrothermal performance of the wall sections with/without vapour-tight/capillary-active insulation under climate change. This paper emphasises comparative analysis between different insulation systems under different weather conditions, aiming to enhance awareness for developing more adaptive and resilient insulation approaches.

2 Methodology

This study consists of two parts: (1) model validation, wherein the simulated hygrothermal responses to the measured boundary conditions from 2019 are compared against the corresponding measured datasets, and (2) comparative simulation, in which three regenerated outdoor weather datasets, along with the measured indoor boundary conditions, are imposed as comparative scenarios.

2.1 Experiment

A set of experimental massive masonry walls in Leuven (Belgium, 50.53° N, 4.42° E) is monitored in detail. The masonry assemblies were constructed with Vandersanden® Robusta bricks (capillary absorption coefficient A_{cap} = 0.61 kg/(m^2·s$^{0.5}$)) and lime mortar (ratios: 12.5 kg Saint-Astier NHL3.5, 50 kg River sand 0/2, 10 L water; A_{cap} = 0.26 kg/(m^2·s$^{0.5}$)) for mould cured mortar), for research on energy efficiency, building performance, historic building retrofitting, etc. The southwest-oriented facade comprises six wall sections separated by well-insulated and vapour-tight wooden frames (Fig. 1). In Belgium, the prevailing wind direction is southwest. Hence, this study focuses on walls exposed to wind-driven rain (Blocken and Carmeliet 2007; Dang et al. 2024a). Wall Sects. 4, 5, and 6 have been hydrophobised externally, whereas wall Sects. 1, 2, and 3 are untreated. In each wall section, two wooden beam ends embedded in the masonry vertically divide the wall into three parts (Fig. 1b–c): the upper and lower parts with multi-dimensional hygrothermal transport, and the middle part where heat and moisture flows are considered one-dimensional. The edge effects are negligible since its height is 3 – 4 times larger than its thickness, and the one-and-a-half-brick-bonded-with-mortar masonry structure can be simplified down to a homogeneous one-dimensional brick (Vereecken and Roels 2013). In this study, only the middle parts of the non-hydrophobized wall Sects. 1, 2, and 3 are analysed. XPS and CSB interior insulation are applied to wall Sects. 1 and 2, respectively, while wall Sect. 3 is uninsulated.

The configurations of the three wall sections are shown in Fig. 2. Abbreviations B, M, X, C, G, and P stand for brick, lime mortar, XPS, CSB, gypsum board and plaster

Fig. 1 The experimental VLIET-building and wall sections: (**a**) & (**b**) exterior view, (**c**) interior view (Source: the authors.)

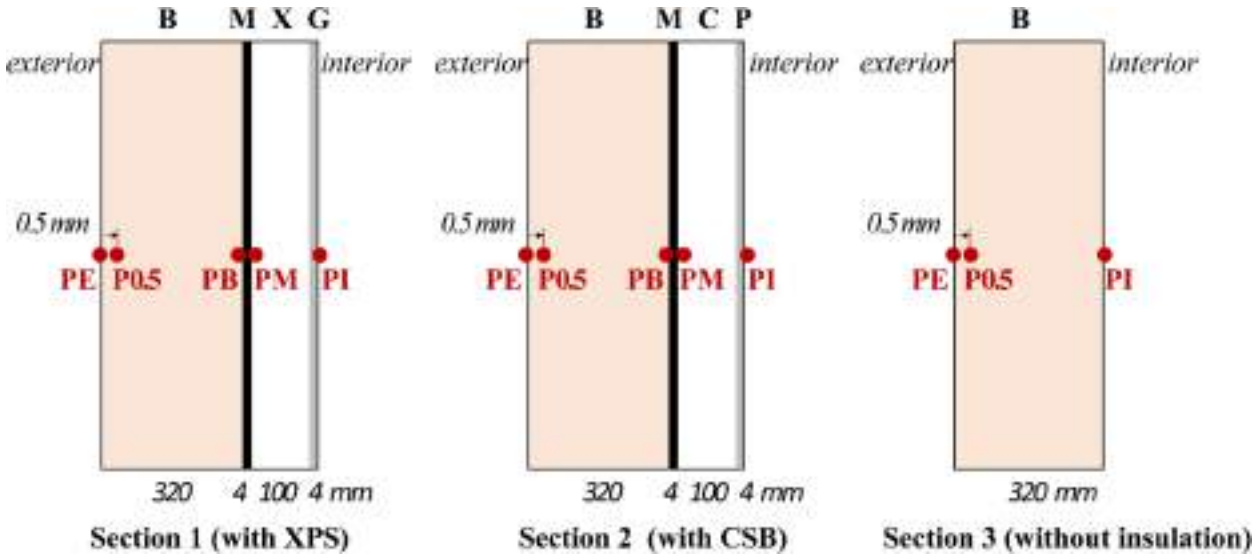

Fig. 2 Configurations of wall sections (Source: the authors.)

layer, respectively. Local temperatures (T, °C) and relative humidity (RH, %) are monitored at several locations: PE (exterior brick surface), P0.5 (0.5 cm from exterior brick surface), PB (interface of brick and mortar), PM (interface of mortar and insulation), and PI (interior surface of finishing layer or brick). The temperature and the relative humidity are measured by in-house calibrated Thermo Electric Type T (class 1) thermocouples and Honeywell HIH-4021 humidity sensors, with an accuracy of ± 0.2 °C and ± 2% RH (Vereecken et al. 2020). A weather station on a flat roof and a meteorological mast in the front free field measure the solar radiation and horizontal rainfall, wind velocity and direction, respectively (Dang et al. 2024a).

Full-scale weather data, encompassing air temperature, relative humidity, wind, precipitation, and solar radiation, have been continuously monitored since June 2018 (Vereecken et al. 2020; Vereecken and Roels 2021b), and the datasets from the year 2019 are used in this study (Fig. 3). The outdoor relative humidity roughly remains above 60% constantly throughout the year, while the indoor relative humidity reaches up to 80% in the summer. The

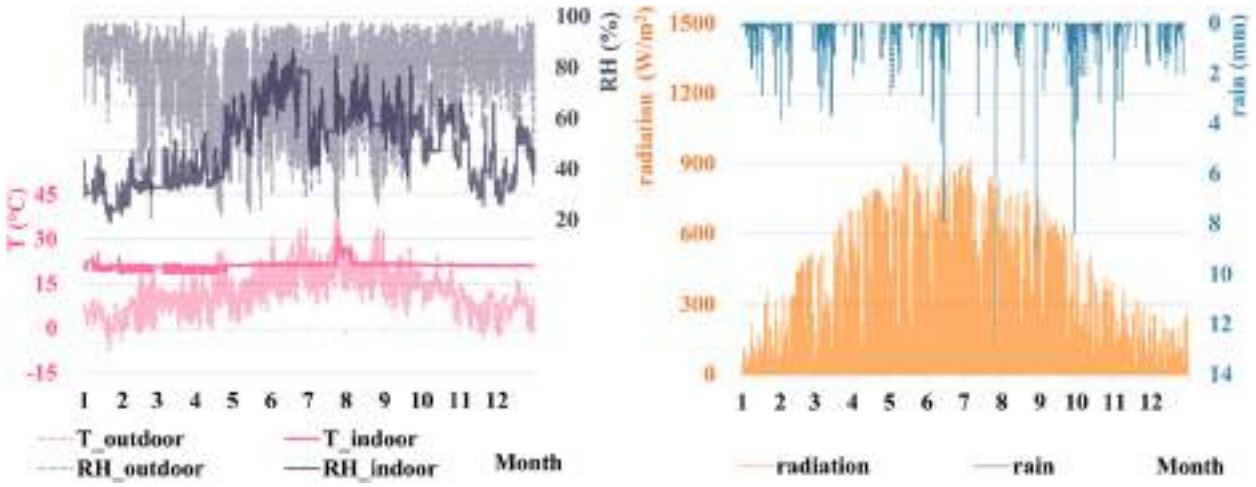

Fig. 3 Monitored weather conditions in 2019 (Source: the authors.)

Table 1 Basic properties of the materials used in the simulation

Materials	ρ [kg/m^3]	$c\rho$ [J/(m^3·K)]	Ψ [m^3/m^3]	λ [W/(m·K)]	μ [-]	A_{cap} [kg/(m^2·s$^{0.5}$)]	w_{sat} [kg/m^3]
Brick 1	1818	840	0.326	0.700	11.6	0.61	210
Brick 2	1852	794	0.301	0.659	12.0	0.26	283
Mortar	1568	488	0.408	0.582	11.4	0.18	405
XPS	40	1500	0.951	0.030	150	0	950
CSB	297	997	0.886	0.068	10.6	0.39	871
Gypsum board	732	1384	0.724	0.211	6.8	0.13	450
Plaster	1498	802	0.435	0.412	9.3	0.02	430

outdoor temperature expresses apparent seasonal variations while the indoor temperature remains around 21 °C. Solar radiation is the highest in summer, while the rain events are more evenly distributed over the year.

The basic properties of the materials used in the simulations are shown in Table 1. The material properties of Brick 1 are measured and translated into the hygrothermal simulation model, DELPHIN (Ren et al. 2019; Feng and Janssen 2021). The other materials (mortar: LehmmoertelLMH_128, XPS: Polystyrene Board Extruded_18, CSB: Remmers Calciumsilikat Schimmelsanierplatte2_592, gypsum board: Rigips Gipskarton_427, plaster: Schaeferkalk Kalkputz SKKP_629) are selected from DELPHIN's material library with the same manufacturers and/or with similar properties. Brick 1 is applied in the validation for a better agreement with the actual conditions, while Brick 2 (Altbauziegel Dresden ZH_496), with a 'medium' capillary absorption coefficient A_{cap} among those in the material library, is selected for the second step simulations to draw more 'general' conclusions. Figure 4 shows the moisture retention curves $w(P_c)$ and liquid permeability curves $K_l(w)$ of the two bricks.

2.2 Simulation

One-dimensional hygrothermal simulations are conducted with DELPHIN 6 (Häupl and Stopp 1987). The governing equations are shown below.

$$\begin{cases} \frac{\partial H(T,P_c)}{\partial t} = \frac{\partial}{\partial x}\left(\lambda \frac{\partial T}{\partial x}\right) + (L_v + c_v T)\frac{\partial}{\partial x}\left(K_v \frac{\partial P_v}{\partial x}\right) + c_l T \frac{\partial}{\partial x}\left(K_l \frac{\partial P_c}{\partial x}\right) & (1) \\ \frac{\partial w(P_c)}{\partial t} = \frac{\partial}{\partial x}\left(K_l \frac{\partial P_c}{\partial x}\right) + \frac{\partial}{\partial x}\left(K_v \frac{\partial P_v}{\partial x}\right) & (2) \end{cases}$$

where c_v and c_l [J/(kg·K)] are specific heat capacity of vapour and liquid respectively; H [J/m^3] is heat density; K_v and K_l [kg/(m·s·Pa)] are vapour and liquid permeability respectively; L_v [J/kg] is the latent heat of evaporation; P_c and P_v [Pa] are capillary pressure and vapour pressure, respectively; T [K] is temperature; t [s] is time; w [kg/m^3] is moisture content; x [m] is distance; λ [W/m·K] is thermal conductivity.

In the first step, the measured outdoor and indoor boundary conditions (Fig. 3) are employed for model validation ("scenario 2019").

In the second step, the weather dataset of a reference year between 2006 and 2020 ("scenario 2006"), derived from the OCCuPANt project (Doutreloup and Fettweis 2021; Doutreloup et al. 2022), is used as the current

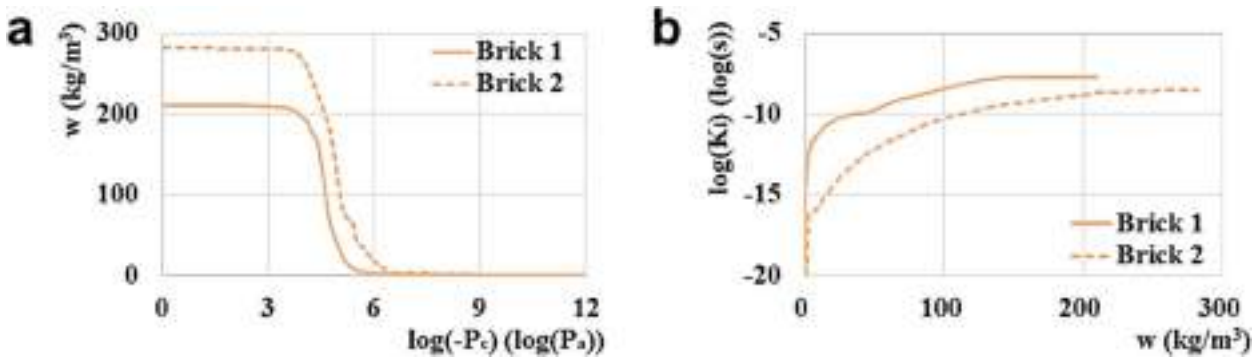

Fig. 4 Moisture retention curves (**a**) and liquid permeability curves (**b**) of the two bricks (Source: the authors.)

scenario, whereas two predicted climate datasets of a reference year between 2061–2080 are applied as the future conditions: "scenario 2061TT" under 'typical' temperature assumption and "scenario 2061ET" under 'extreme' temperature assumption with the most extreme outliers. The 'typical' climate datasets are based on the frequency representative typical months (Barnaby and Crawley 2012) from the available long-term (> 10 years) observations or modelled data by using Finkelstein–Schafer statistics (Finkelstein and Schafer 1971). The 'extreme' climate datasets are formed by selecting the most extreme outliers instead of typical data (Ferrari and Lee 2008). The socioeconomic pathway SSP370, characterised by a high greenhouse gas emission mode at an upper-middle level with an additional solar irradiation of 7 W/m^2 by the year 2100 as calculated by the Max Planck Institute, is assumed in the simulation. The three scenarios are assumed to be comparable, and the only uncertainty is the systematic error subjected to the calculation method for future climate generation, which is not within the scope of this paper. The monitored indoor datasets in 2019 are still employed as indoor boundary conditions.

Table 2 shows the hourly outdoor temperature, relative humidity, global horizontal solar radiation, and horizontal rain of the scenarios 2006, 2061TT, and 2061ET, with measured datasets in 2019 as a reference. The outdoor temperature in 2019 is relatively higher than that of the scenario in 2006, as representative of the recent 15 years. The average relative humidity exceeds 75% among the three scenarios. The future solar radiation under scenarios 2061TT and 2061ET is slightly higher than the scenario 2006. Annual precipitation in scenario 2061ET is much higher than in scenario 2006 by over 300 mm, and the additional rain events mainly take place from January to March and from October to November. Figures 5, 6, 7 and 8 show the hourly and daily average or total temperature, relative humidity, global horizontal solar radiation, and horizontal rain for the three scenarios.

Surface heat transfer coefficients 8 and 17 W/(m^2·K) are allocated to the interior and exterior surfaces,

Table 2 Data features of the outdoor temperature, relative humidity, global horizontal solar radiation, and precipitation of the scenarios 2019, 2006, 2061TT, and 2061ET

Year/scenario	T_{max} [°C]	T_{min} [°C]	T_{avg} [°C]	RH_{max} [%]	RH_{min} [%]	RH_{avg} [%]	Total radiation [kWh/m^2]	Total rain [mm]
2019	41.3	-7.5	12.0	99.3	20.3	76.5	1.118E+06	732.2
2006	34.6	-17.5	11.3	100.0	24.9	81.3	1.078E+06	699.0
2061TT	38.3	-6.9	12.6	100.0	26.2	80.3	1.118E+06	705.9
2061ET	40.0	-1.3	14.9	100.0	21.0	77.6	1.101E+06	1022.0

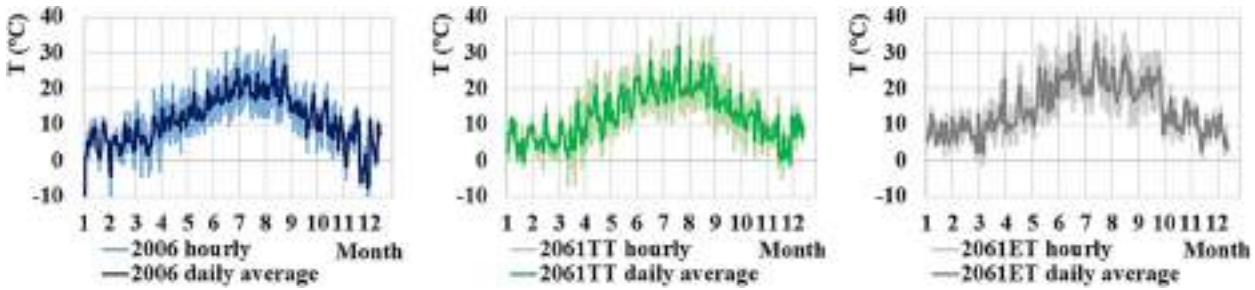

Fig. 5 Outdoor temperature of the scenarios 2006, 2061TT, and 2061ET (Source: the authors.)

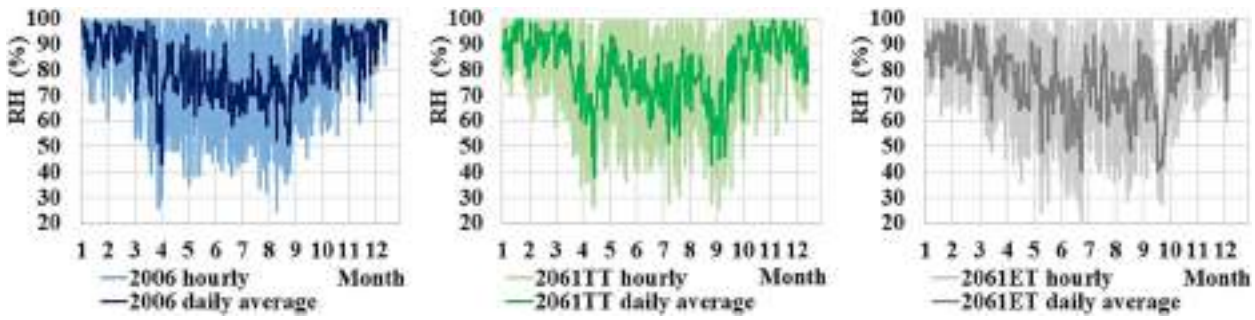

Fig. 6 Outdoor relative humidity of the scenarios 2006, 2061TT, and 2061ET (Source: the authors.)

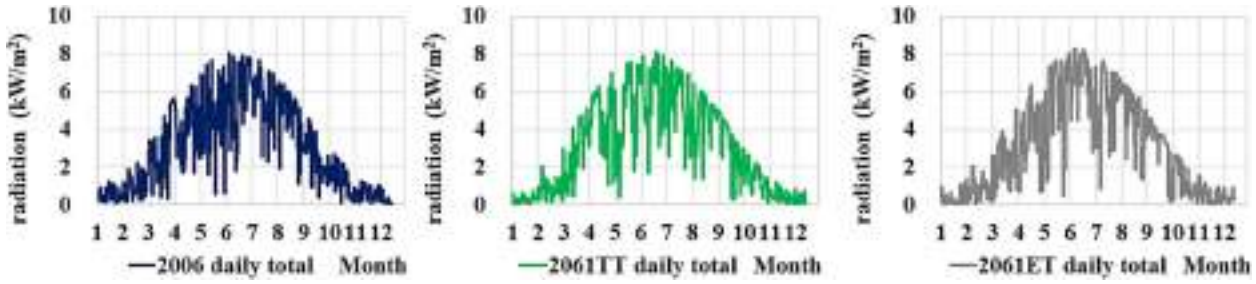

Fig. 7 Global horizontal solar radiation of the scenarios 2006, 2061TT, and 2061ET (Source: the authors.)

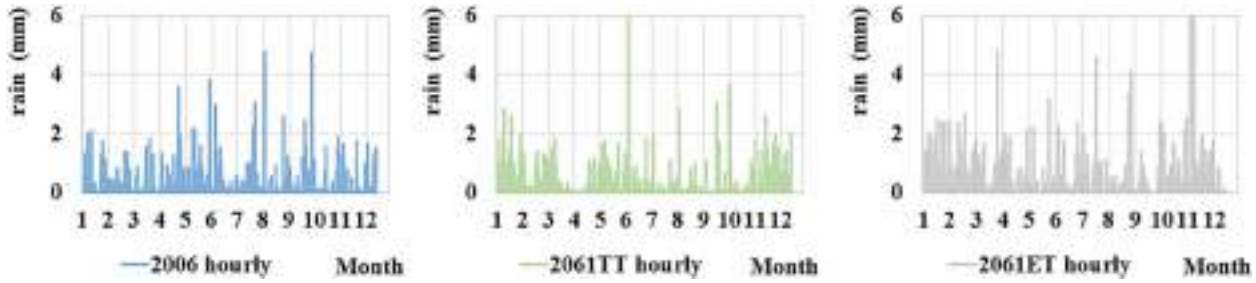

Fig. 8 Horizontal rain of the scenarios 2006, 2061TT, and 2061ET (Source: the authors.)

respectively, while the surface vapour transfer coefficients are set at 5.6×10^{-8} and 1.19×10^{-7} s/m for interior and exterior surfaces, respectively (DIN 4108[4]). Initial conditions are given at 10 °C and 90% for the structure. The meshes are finely discretised for a grid-independent solution. The simulation runs for a three-year cycle, and the last-year results are analysed. The output time step is set as 1 h.

3 Results and discussion

Section 3.1 presents the model validation, and the comparative simulation results are discussed in Sects. 3.2 through 3.5. Four indicators are employed to evaluate the hygrothermal performance and associated environmental risks. Moisture profiles provide a clear representation of the tempo-spatial distribution of moisture saturation within pores, which is directly related to moisture-related failures. The assessment of mould growth risks involves the comparison of paired simulated temperatures and relative humidity values against established thresholds for mould spore germination. The risks of frost damage are determined by the combined effects of sufficient moisture levels within pores and nearly-zero local temperatures. Heat losses indicate the effectiveness of insulation materials in enhancing energy efficiency.

3.1 Model validation

Model validation is a prerequisite for a reliable application of hygrothermal simulations. The model can be considered validated if similar trends and/or limited deviations are observed between simulated and measured results (Dang, Janssen, and Roels 2023b, 2024b). Simulated temperature and relative humidity at the brick-insulation interfaces are confronted with measured data to validate the simulation model.

The simulated local temperature and relative humidity at PM of wall Sects. 1 and 2 and PI of wall Sect. 3 under scenario 2019 both agree with the measured data (Fig. 9). Although there are no criteria of critical values, a small root-mean-square-error indicates the reliability of the simulation. Since the measured boundary conditions are reproduced, the differences among the moisture storage and transport properties of the actual applied materials and those from DELPHIN's material library, differences between the implemented and actual surface transport coefficients, and the simplification of the masonry structure may all contribute to the deviations. Considering the overall trends of the simulated and measured results are consistent, the model is assumed to be sufficiently robust and capable for further comparative analysis.

[4] DIN 4108 is a standard titled '*Wärmeschutz und Energie-Einsparung in Gebäuden*' (Thermal insulation and energy saving in buildings), which was developed under the direction of the German Institute for Standardization (DIN).

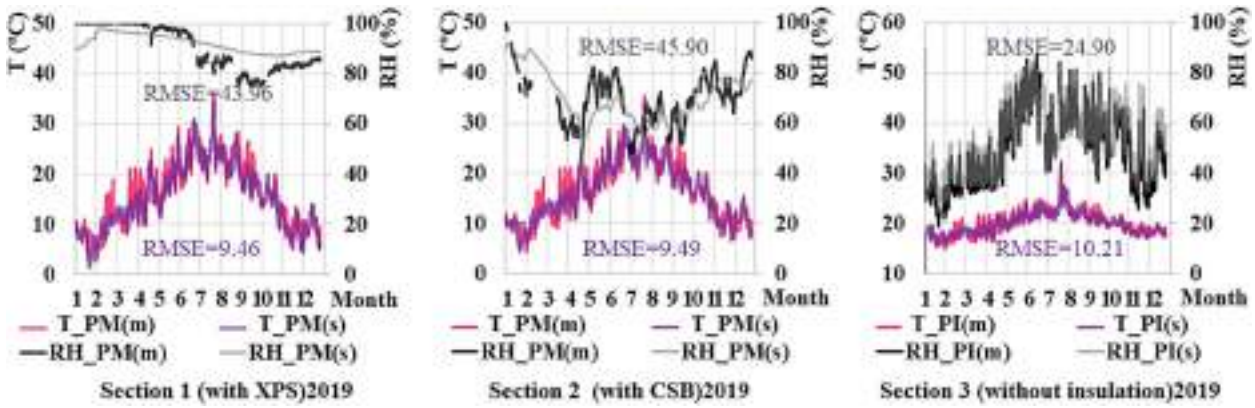

Fig. 9 Model validation: measurement (m) versus simulation (s) (Source: the authors.)

3.2 Moisture profiles

Moisture profiles visually represent how moisture saturates the pores of building materials over time and space and directly correlates with degradation and damage. Figure 10 shows the time series of moisture profiles of the wall sections under the three scenarios. Each row and each column of the graphs indicate the same wall section and the same scenario, respectively. The horizontal axis represents the time in months, while the vertical axis shows the spatial configurations (see Fig. 2). The 'bluer' the figure is, the higher the moisture content will be. All the wall sections have been undersaturated over the year in the current scenario, while the moisture content has significantly increased in future scenarios, particularly in the 2061ET scenario. The low moisture permeance of XPS constantly leads to the highest moisture content in all scenarios. CSB, exhibiting a reduced vapour transport resistance and an elevated capillary absorption coefficient in comparison to XPS (see Table 1), facilitates the flow of moisture. This results in a partial reduction of moisture content, leading to a performance of the wall section that is akin to that of uninsulated structures.

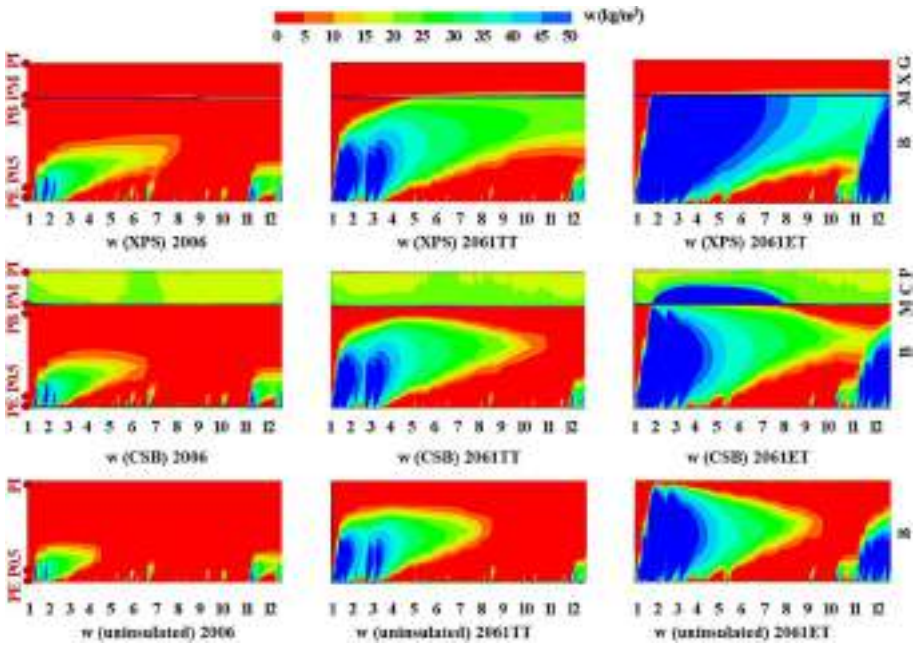

Fig. 10 Time series of moisture profiles of scenarios 2006, 2061TT, and 2061ET (Source: the authors.)

3.3 Mould growth risks

Mould growth serves as an indicator of biological failures. The dependent factors for mould spores to germinate and proliferate include temperature, relative humidity, pH, lighting, etc. (Vereecken and Roels 2012). Particularly, relative humidity over 75% provides optimal conditions (Heseltine and Rosen 2009), while moderate temperature accelerates the process. Generalised isopleths for spore germination proposed by Sedlbauer (2001) are employed to evaluate mould growth risks. A combination of temperature and relative humidity at a specific position is plotted. More points lying above the critical lines indicate more serious biological growth risks. The indications in days refer to the mould spore germination time. Hourly temperature and relative humidity data of the interior brick surface cells (PB in wall Sects. 1 and 2, and PI in wall Sect. 3) are plotted in Fig. 11. There are overly high points for the XPS insulated wall than for the CSB insulated wall, but both internal insulation systems increase the mould growth risks. In future scenarios, more points are in the risky zones, including those between 0 and 10 °C which are risk-free in scenario 2006. It may indicate that warm winter can increase mould growth risks, especially for the wall with a vapour-tight insulation system. Although mould growth is inevitable in the insulated brick walls in summer, a vapour-open system that allows outward moisture drying can reduce the relative humidity and, therefore, the mould growth risks. In the extreme temperature scenario, 2061ET, even the CSB-insulated wall is predominant in the high-risk zone, whereas the risk to the uninsulated wall is reduced.

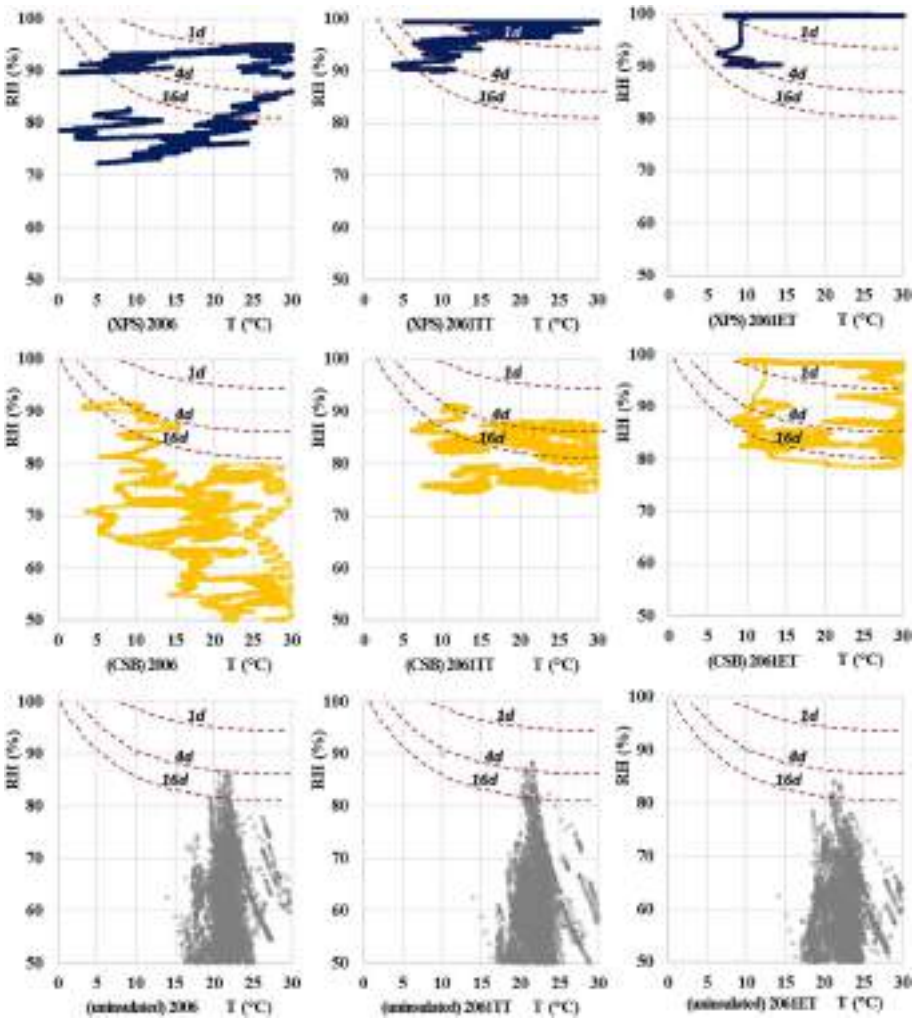

Fig. 11 Mould spore germination isopleths of interior brick surfaces under scenarios 2006, 2061TT, and 2061ET (Source: the authors.)

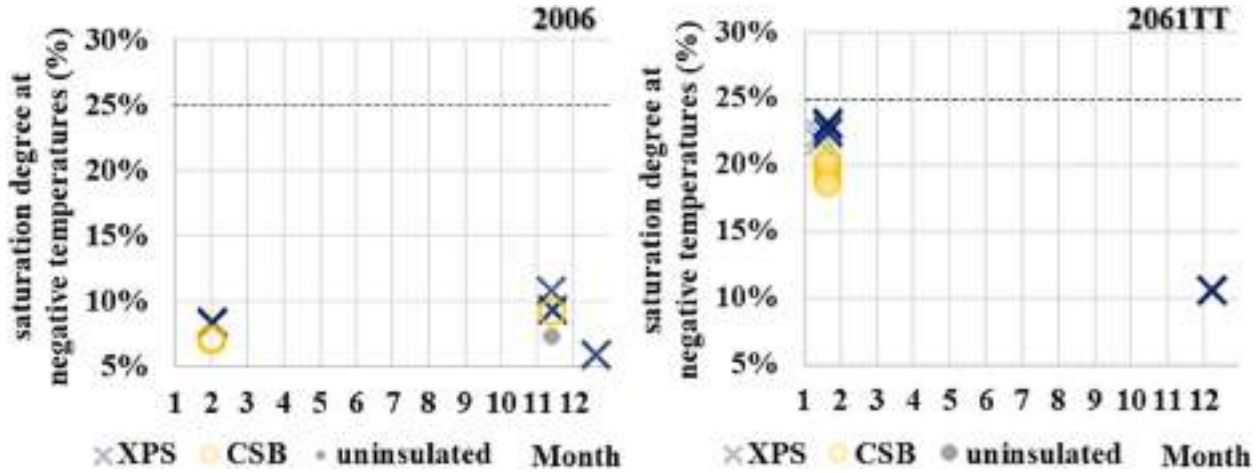

Fig. 12 Moisture saturation degrees at 0.5 cm from the exterior surface (P0.5) at negative temperatures under scenarios 2006 and 2061TT (Source: the authors.)

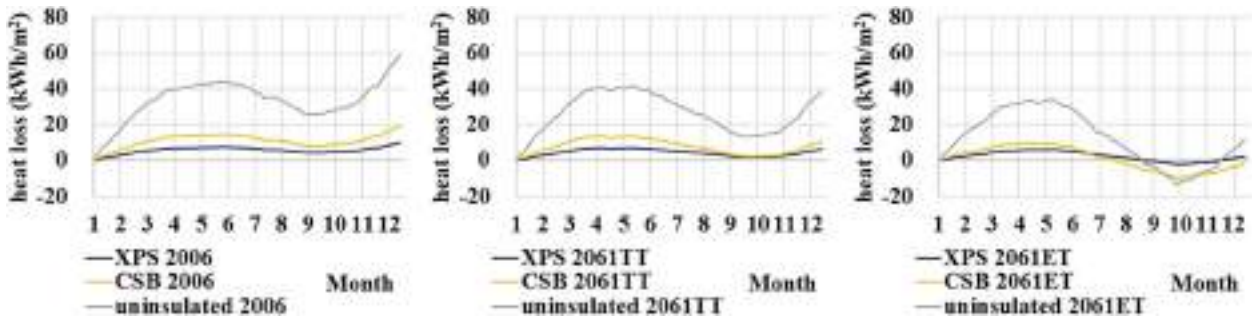

Fig. 13 Cumulative heat loss under scenarios 2006, 2061TT and 2061ET (Source: the authors.)

3.4 Frost damage risks

Frost damage from moisture volumetric changes during freeze–thaw cycles within pores can lead to cracks, flaking, and other structural deteriorations (Zhou et al. 2017). The criteria proposed by Mensinga, Straube, and Schumacher (2010) are adopted. When the local temperature at 0.5 cm from the exterior surface fluctuates around zero degrees and the moisture mass is larger than a quarter of the saturated moisture content, the material is assumed to experience frost damage (Vereecken et al. 2015; Tijskens et al. 2019). Although the annual precipitation in scenario 2061ET is the largest, the outdoor temperature and, therefore, the temperature at 0.5 cm only seldom goes below zero degrees in winter. Moisture contents at 0.5 cm from the exterior surface (P0.5) at negative temperatures stay below 25% of the saturated moisture content (283 kg/m^3, see Table 1) in scenarios 2006 and 2061TT (Fig. 12). This indicates that frost damage does not occur in both current and future scenarios. Among the three, the saturation degree of wall Sect. 1 (XPS) is higher than wall Sect. 2 (CSB), followed by wall Sect. 3 (uninsulated). In other words, a vapour-tight insulation system might more likely cause frost damage on bricks with smaller moisture storage capacity in colder and moister weather conditions.

3.5 Heat losses

Figure 13 presents a comparison of the cumulative heat losses (heat fluxes from indoor to outdoor environment) across the three scenarios. Internal insulation systems significantly reduce heat losses. Particularly in scenarios 2006 and 2061TT, the annual heat loss of the wall insulated with XPS reduces nearly 85% that of the uninsulated wall. There is a significant decreasing trend between the current and future heat losses, possibly due to the increasing heat gains from solar radiation.

4 Conclusion

This paper compares the hygrothermal response of vapour-tight and capillary-active insulated masonry walls in Leuven, Belgium, under current and future climate conditions.

The main findings and insights are:

(1) Calcium silicate board, with higher vapour and liquid moisture transport coefficients, can effectively facilitate the inward moisture flow and, therefore, reduce the risks of mould growth, frost damage and other moisture-related problems. A masonry wall with a capillary-active internal insulation system behaves more similarly to the uninsulated wall than the one with vapour-tight insulation.
(2) The current and future climate conditions considerably influence the hygrothermal response of the building components. It is unavoidable that there will be more serious risks of mould growth in the internally insulated walls when high relative humidity conditions are presented, for instance, even during summer in the future with expected larger precipitation. The positive effects of the capillary-active insulation system will be reduced, while the uninsulated wall will not show higher damage risks. Frost damage mainly depends on sufficient moisture storage, low temperature, and large precipitation. None of the wall sections resulted in frost damage for all scenarios, although the vapour-tight insulation has a slightly higher risk.
(3) Both vapour-tight and capillary-active insulation can improve the energy efficiency. Although the vapour-tight insulation system performs slightly better, the actual improvement at the building scale might be minimal. Overall, practitioners should always learn more about the hygrothermal properties of the insulation materials and their responses to the changing climates to balance between energy efficiency and moisture safety.

The limitations and expectations are:

(1) It is complex to measure at all desired positions for longer periods, but knowing more details about how a building structure behaves under different weather conditions is highly required. Future climate is subject to various factors, including geographical locations and greenhouse gas emissions. More climate scenarios should be considered to draw a more general conclusion on the hygrothermal response of the two internal insulation systems.
(2) Different production methods and exposure conditions resulted in a variety of historic building materials and, therefore, require a deeper analysis of the material properties. Admittedly, the behaviours of the specific XPS and CSB materials involved in this study may not be applied to all possible vapour-tight and capillary-active insulation materials. In further evaluations, a wider range of bricks (including those in the material library of the simulation models and measured material properties) should be included, while more 'capillary active' insulation materials under other weather conditions should be involved in probabilistic and sensitivity analysis for a more generalised conclusion.
(3) Hygrothermal behaviours of building components under future climates are full of uncertainties. Researchers should delve into the hygrothermal behaviour of the insulation materials, the hygrothermal response of the original facades, and weather conditions, providing engaging insights into the practitioners' decision-making in the adaptive reuse of historical buildings.

Abbreviations

English

A	Absorption coefficient, kg/(m^2·s$^{0.5}$)
c	Specific heat capacity, J/(kg·K)
H	Heat density, J/m^3
L_v	Latent heat of evaporation, J/kg
K	Permeability, kg/(m·s·Pa)
P	Pressure, Pa
RH	Relative humidity, %
T	Temperature, °C
t	Time, s
w	Moisture content, kg/m^3
x	Distance, m

Greek

λ	Thermal conductivity, W/(m·K)
μ	Vapour diffusion resistance factor, -
ρ	Density, kg/m^3
Ψ	Porosity, m^3/m^3

Subscripts

avg	Average
c	Capillary
cap	Capillary saturation
l	Liquid
max	Maximum
min	Minimum
sat	Saturation
v	Vapour

Acknowledgements
Not applicable.

Authors' contributions
Xinyuan Dang made substantial contributions to the conception design, the acquisition, analysis, interpretation of data, and drafted the work. Evy Vereecken, Hans Janssen, and Staf Roels contributed to conception design, data interpretation and manuscript revisions. All authors read and approved the final manuscript.

Funding
The research is supported by China Scholarship Council (NO. 202006090005).

Data availability
Not applicable.

Declarations

Ethics approval and consent to participate
Not applicable.

Consent for publication
Not applicable.

Competing interests
The author declare that they have no competing interests.

Received: 22 May 2023 Revised: 4 March 2025 Accepted: 17 March 2025
Published online: 31 March 2025

References

Abuku, Masaru, Bert Blocken, and Staf Roels. 2009. Moisture response of building facades to wind-driven rain: Field measurements compared with numerical simulations. *Journal of Wind Engineering and Industrial Aerodynamics* 97 (5–6): 197–207.

Barnaby, Charles S., and Drury B. Crawley. 2012. Weather data for building performance simulation. In *Building performance simulation for design and operation*, 61–79. London: Routledge.

Berardi, Umberto. 2017. The impact of temperature dependency of the building insulation thermal conductivity in the Canadian climate. *Energy Procedia* 132: 237–242.

Biseniece, Ed.īte, Gatis Žogla, Agris Kamenders, Reinis Purviņš, Kristaps Kašs, Ruta Vanaga, and Andra Blumberga. 2017. Thermal performance of internally insulated historic brick building in cold climate: A long term case study. *Energy and Buildings* 152: 577–586.

Blocken, Bert, and Jan Carmeliet. 2007. Validation of CFD simulations of wind-driven rain on a low-rise building facade. *Building and Environment* 42 (7): 2530–2548.

Blumberga, Andra, Kristaps Kašs, Edīte Kamendere, Gatis Žogla, Agris Kamenders, Dagnija Blumberga, and Armands Grāvelsiņš et al. 2016. *State of the art on historic building insulation materials and retrofit strategies*. http://ribuild-web.sbi.aau.dk/sites/default/files/RIBuild_D1.2_1.0.pdf.

Bottino-Leone, Dario, Marco Larcher, Daniel Herrera-Avellanosa, Franziska Haas, and Alexandra Troi. 2019. Evaluation of natural-based internal insulation systems in historic buildings through a holistic approach. *Energy* 181: 521–531.

Curtis, Roger. 2010. Climate change and traditional buildings: The approach taken by Historic Scotland. *Journal of Architectural Conservation* 16 (3): 7–27.

Dang, Xinyuan, Shuichi Hokoi, Yonghui Li, Changchang Xia, and Ma Yan. 2019. Evaluation of mould growth risks due to air leakage through air cavity of the building walls. *MATEC Web of Conferences* 282: 02060. https://www.matec-conferences.org/articles/matecconf/pdf/2019/31/matecconf_cesbp2019_02060.pdf.

Dang, Xinyuan, Hans Janssen, and Staf Roels. 2023a. Comparative simulations on hygrothermal performance of calcium silicate and wood fiber as capillary active internal insulation materials. Paper presented at the 2nd International Conference on Moisture in Buildings, online, July 3–4. *ScienceOpen*. https://doi.org/10.14293/ICMB230020.

Dang, Xinyuan, Hans Janssen, and Staf Roels. 2023b. Hygrothermal Modelling of one-dimensional Wall Assemblies: inter-model Validation between WUFI and DELPHIN. *Journal of Physics: Conference Series* 2654 (1): 012040.

Dang, Xinyuan, Evy Vereecken, Hans Janssen, and Staf Roels. 2024a. Impact of semi-empirical methods implemented in heat, air, and moisture (HAM) models on predicted wind-driven rain (WDR) loads and hygrothermal responses. *Building and Environment* 262: 111770.

Dang, Xinyuan, Hans Janssen, and Staf Roels. 2024b. A comprehensive benchmark dataset for the validation of building component heat, air, and moisture (HAM) models. *Building Simulation* 17: 1893–1907.

Dang, Xinyuan, Hans Janssen, and Staf Roels. 2025a. User impact as an uncertainty in hygrothermal simulations: insights from a round robin test. In *Multiphysics and Multiscale Building Physics—Proceedings of the 9th International Building Physics Conference (IBPC 2024) Volume 1: Moisture and Materials*, ed. U. Berardi, 68–75. Springer Singapore. https://doi.org/10.1007/978-981-97-8305-2_9.

Dang, Xinyuan, Ana Sofia Guimarães, Andreas Sarkany, Anssi Laukkarinen, Bingyu Xu, Bruno Vanderschelden, Carsten Rode et al. 2025b. A state-of-the-art empirical round robin validation of heat, air and moisture (HAM) models. Building and Environment 112867.

Delgado, João MPQ, Eva Barreira, Nuno MM Ramos, and Vasco Peixoto de Freitas. 2012. *Hygrothermal numerical simulation tools applied to building physics*. London: Springer.

Desta, Tadiwos Zerihun, Jelle Langmans, and Staf Roels. 2011. Experimental data set for validation of heat, air and moisture transport models of building envelopes. *Building and Environment* 46 (5): 1038–1046.

Dong, Yitong, Jiashu Kong, Seyedmostafa Mousavi, Behzad Rismanchi, and Pow-Seng. Yap. 2023. Wall insulation materials in different climate zones: A review on challenges and opportunities of available alternatives. *Thermo* 3 (1): 38–65.

Doutreloup, Sébastien, and Xavier Fettweis. 2021. Typical & Extreme Meteorological Year and Heatwaves for Dynamic Building Simulations in Belgium based on MAR model Simulations (version 1.0. 0). Genève : Zenodo.

Doutreloup, Sébastien., Xavier Fettweis, Ramin Rahif, Essam Elnagar, Mohsen S. Pourkiaei, Deepak Amaripadath, and Shady Attia. 2022. Historical and future weather data for dynamic building simulations in Belgium using the regional climate model MAR: Typical and extreme meteorological year and heatwaves. *Earth System Science Data* 14 (7): 3039–3051.

Drdácký, Miloš F. Flood damage to historic buildings and structures. 2010. *Journal of Performance of Constructed Facilities* 24 (5): 439–445.

Erkal, Aykut, Dina D'Ayala, and Lourenço Sequeira. 2012. Assessment of wind-driven rain impact, related surface erosion and surface strength reduction of historic building materials. *Building and Environment* 57: 336–348.

Feng, Chi, and Hans Janssen. 2021. Hygric properties of porous building materials (VII): Full-range benchmark characterizations of three materials. *Building and Environment* 195: 107727.

Finkelstein, Jack M., and Ray E. Schafer. 1971. Improved goodness-of-fit tests. *Biometrika* 58 (3): 641–645.

Ferrari, David, and Trevor Lee. 2008. Beyond TMY: climate data for specific applications. In *Proceedings 3rd International Solar Energy Society conference–Asia Pacific region (ISES-AP-08), Sydney, November 25–28*.

Gan, Weinan, Xiaolong Li, Jinzhong Fang, and Chi Feng. 2025. Influence of input uncertainty on the 1-D hygrothermal simulation of composite walls in China. *Building Simulation* 18: 19–32. https://doi.org/10.1007/s12273-024-1204-8.

Grunewald, John, U. Ruisinger, and P. Häupl. 2020. The Rijksmuseum Amsterdam–hygrothermal analysis and dimensioning of thermal insulation. In *Research in building physics and building engineering: 3rd International Conference in Building Physics (Montreal, Canada, 27-31 August 2006)*, eds. Paul Fazio, Hua Ge, Jiwu Rao, Guylaine Desmarais, 345–352. Boca Raton: CRC Press.

Häupl, Peter, and Horst Stopp. 1987. Feuchtetransport in Baustoffen und Bauwerksteilen. PhD diss., Technische Universität Dresden.

Hamid, Akram Abdul, and Petter Wallentén. 2017. Hygrothermal assessment of internally added thermal insulation on external brick walls in Swedish multifamily buildings. *Building and Environment* 123: 351–362.

Harrestrup, Maria, and Svend Svendsen. 2015. Full-scale test of an old heritage multi-storey building undergoing energy retrofitting with focus on internal insulation and moisture. *Building and Environment* 85: 123–133.

Héberlé, Elodie, and Burgholzer Julien. 2016. Guidance for Finding a Sustainable Balance between Energy Efficiency, Comfort, Moisture Damage and Cultural Heritage Value in Historic Buildings. In *EECHB-2016: Second International Conference on Energy Efficiency and Comfort of Historic Buildings*, eds. Michael de Bouw, Samuel Dubois, Liesbeth Dekeyser and Yves Vanhellemont, 52–58. Brussels: Flanders Heritage Agency. https://www.eechb.eu/wp-content/uploads/2016/12/Proceedings_EECHB.pdf.

Heseltine, Elisabeth, and Jerome Rosen, eds. 2009. *WHO guidelines for indoor air quality: dampness and mould*. Mülheim an der Ruhr: Druckpartner Moser.

Huang, Huakun, Yijun Zhou, Renda Huang, Huijun Wu, Yongjun Sun, Gongsheng Huang, and Tao Xu. 2020. Optimum insulation thicknesses and energy conservation of building thermal insulation materials in Chinese zone of humid subtropical climate. *Sustainable Cities and Society* 52: 101840.

Janssens, Kaat, Chi Feng, Valentina Marincioni, and Nathan Van Den Bossche. 2024. Comparison of different frost models with hygrothermal

simulations to better understand frost damage in porous building materials. *Building and Environment* 225(1): 111399.
Klõšeiko, Paul, Endrik Arumägi, and Targo Kalamees. 2015. Hygrothermal performance of internally insulated brick wall in cold climate: A case study in a historical school building. *Journal of Building Physics* 38 (5): 444–464.
Klõšeiko, Paul, and Targo Kalamees. 2022. Hygrothermal performance of a brick wall with interior insulation in cold climate: Vapour open versus vapour tight approach. *Journal of Building Physics* 46 (1): 3–35.
Lalesca Aparecida da Guarda, Emeli, Elaise Gabriel, Renata Mansuelo Alves Domingos, Luciane Cleonice Durante, Ivan Julio Apolonio Callejas, João Carlos Machado Sanches, and Karyna de Andrade Carvalho Rosseti. 2019. Adaptive comfort assessment for different thermal insulations for building envelope against the effects of global warming in the mid-western Brazil. *IOP Conference Series: Earth and Environmental Science* 329 (1): 012057.
Lång, Lukas, Patrik Johansson, Carl-Magnus Capener, Hans Janssen, Jelle Langmans, Eva B. Møller, Marco D'Orazio, and Enrico Quagliarini. 2018. Outlining a methodology for assessing deterioration threshold criteria: Linked to retrofitting historical buildings with internal insulation. In *Proceedings 3rd International Conference on Energy Efficiency in Historic Buildings (EEHB2018)*, 32–40.
Langmans, Jelle, Tadiwos Z. Desta, Lieven Alderweireldt, and Staf Roels. 2016. Field study on the air change rate behind residential rainscreen cladding systems: A parameter analysis. *Building and Environment* 95: 1–12.
Lassandro, Paola, and Silvia Di Turi. 2017. Façade retrofitting: from energy efficiency to climate change mitigation. *Energy Procedia* 140: 182–193.
Lisitano, Ivana Mattea, Deborah Laggiard, Stefano Fantucci, Valentina Serra, and Elisa Fenoglio. 2021. Evaluating the Impact of Indoor Insulation on Historic Buildings: A Multilevel Approach Involving Heat and Moisture Simulations. *Applied Sciences* 11 (17): 7944.
Li, Yonghui, Xinyuan Dang, Changchang Xia, Yan Ma, Daisuke Ogura, and Shuichi Hokoi. 2020. The Effect of Air leakage through the Air Cavities of Building Walls on Mould Growth Risks *Energies* 13 (5): 1177.
Lu, Jacqueline, Valentina Marincioni, Scott Allan Orr, and Hector Altamirano-Medina. 2021. Climate resilience of internally-insulated historic masonry assemblies: Comparison of moisture risk under current and future climate scenarios. *Minerals* 11 (3): 271.
Mensinga, Peter, John Straube, Christopher Schumacher. 2010. Assessing the freeze-thaw resistance of clay brick for interior insulation retrofit projects. In *Proceedings of the XI International Conference Thermal Performance of the Exterior Envelopes of Whole Buildings, Clearwater, FL, USA*, 5–9. https://web.ornl.gov/sci/buildings/conf-archive/2010%20B11%20papers/203_Mensinga.pdf.
Nik, Vahid M. 2017. Application of typical and extreme weather data sets in the hygrothermal simulation of building components for future climate–A case study for a wooden frame wall. *Energy and Buildings* 154: 30–45.
Panico, Simone, Marco Larcher, Valentina Marincioni, Alexandra Troi, Cristina Baglivo, and Paolo Maria Congedo. 2023. Identifying key parameters through a sensitivity analysis for realistic hygrothermal simulations at wall level supported by monitored data. *Building and Environment* 229: 109969.
Posani, Magda, Maria Do Rosario Veiga, and Vasco Peixoto de Freitas. 2021. Towards resilience and sustainability for historic buildings: A review of envelope retrofit possibilities and a discussion on hygric compatibility of thermal insulations. *International Journal of Architectural Heritage* 15 (5): 807–823.
Ren, Peng, Chi Feng, and Hans Janssen. 2019. Hygric properties of porous building materials (V): Comparison of different methods to determine moisture diffusivity. *Building and Environment* 164: 106344.
Rosas-Flores, Jorge Alberto, and Dionicio Rosas-Flores. 2020. Potential energy savings and mitigation of emissions by insulation for residential buildings in Mexico. *Energy and buildings* 209: 109698.
Rose, William B. 2005. Should the walls of historic buildings be insulated?. *APT bulletin* 36 (4): 13–18.
Sathiparan, Navaratnarajah, and Udayakumar Rumeshkumar. 2018. Effect of moisture condition on mechanical behavior of low strength brick masonry. *Journal of Building Engineering* 17: 23–31.
Sedlbauer, Klaus. 2001. Prediction of mould fungus formation on the surface of and inside building components. *Fraunhofer Institute for Building Physics* 9 (2): 75–141.
Stazi, Francesca, Ambra Vegliò, Costanzo Di Perna, Placido Munafò. 2013. Experimental comparison between 3 different traditional wall constructions and dynamic simulations to identify optimal thermal insulation strategies. *Energy and buildings* 60: 429–441.
Tijskens, Astrid, Staf Roels, and Hans Janssen. 2019. Neural networks for metamodelling the hygrothermal behaviour of building components. *Building and Environment* 162: 106282.
Tingley, Danielle Densley, Abigail Hathway, and Buick Davison. 2015. An environmental impact comparison of external wall insulation types. *Building and Environment* 85 (2015): 182–189.
Vandemeulebroucke, Isabeau, Bruno Vanderschelden, Kaat Janssens, Steven Caluwaerts, Nathan Van Den Bossche. 2024. The impact of climate change on degradation in historical building envelopes: Progress in research using hygrothermal models. *Journal of Cultural Heritage* 70 (November–December): 345–363. https://doi.org/10.1016/j.culher.2024.10.005.
Vereecken, Evy, and Staf Roels. 2012. Review of mould prediction models and their influence on mould risk evaluation. *Building and Environment* 51: 296–310.
Vereecken, Evy, and Staf Roels. 2013. Hygric performance of a massive masonry wall: How do the mortar joints influence the moisture flux? *Construction and Building Materials* 41: 697–707.
Vereecken, Evy, Liesje Van Gelder, Hans Janssen, and Staf Roels. 2015. Interior insulation for wall retrofitting–A probabilistic analysis of energy savings and hygrothermal risks. *Energy and Buildings* 89: 231–244.
Vereecken, Evy, and Staf Roels. 2016. Capillary active interior insulation systems for wall retrofitting: A more nuanced story. *International Journal of Architectural Heritage* 10 (5): 558–569.
Vereecken, Evy, Daan Deckers, Hans Janssen, and Staf Roels. 2020. Field study on hydrophobised internally insulated masonry walls. Paper presented in XV International Conference on Durability of Building Materials and Components (DBMC 2020), Barcelona, October 20–23. https://doi.org/10.23967/dbmc.2020.067.
Vereecken, Evy, and Staf Roels. 2021a. Internally insulated walls with embedded wooden beams: how does hydrophobisation change the hygric performance? Paper presented in 1st International Conference on Moisture in Buildings 2021, online, June 28–29.
Vereecken, Evy, and Staf Roels. 2021b. Hygrothermal performance of internally insulated masonry walls with embedded wooden beam heads: a field study on the impact of hydrophobisation. *Journal of Physics: Conference Series* 2069 (1): 012019.
Vitiello, Veronica, Roberto Castelluccio, and Mercedes Del Rio Merino. 2020. Experimental research to evaluate the percentage change of thermal and mechanical performances of bricks in historical buildings due to moisture. *Construction and Building Materials* 244: 118107.
Walker, Rosanne, and Sara Pavía. 2018. Thermal and moisture monitoring of an internally insulated historic brick wall. *Building and Environment* 133: 178–186.
Yuan, Jihui, Craig Farnham, and Kazuo Emura. 2017. Optimal combination of thermal resistance of insulation materials and primary fuel sources for six climate zones of Japan. *Energy and Buildings* 153: 403–411.
Zhou, Xiaohai, Dominique Derome, and Jan Carmeliet. 2017. Hygrothermal modeling and evaluation of freeze-thaw damage risk of masonry walls retrofitted with internal insulation. *Building and Environment* 125: 285–298.
Zhou, Xiaohai, Jan Carmeliet, and Dominique Derome. 2020. Assessment of risk of freeze-thaw damage in internally insulated masonry in a changing climate. *Building and Environment* 175: 106773.
Zhu, Panyu, Volker Huckemann, and M. Norbert Fisch. 2011. The optimum thickness and energy saving potential of external wall insulation in different climate zones of China. *Procedia Engineering* 21: 608–616.

Publisher's Note